RSC Advances

RSC Advances

www.rsc.org/advances

ROYAL SOCIETY
OF CHEMISTRY

www.rsc.org/advances
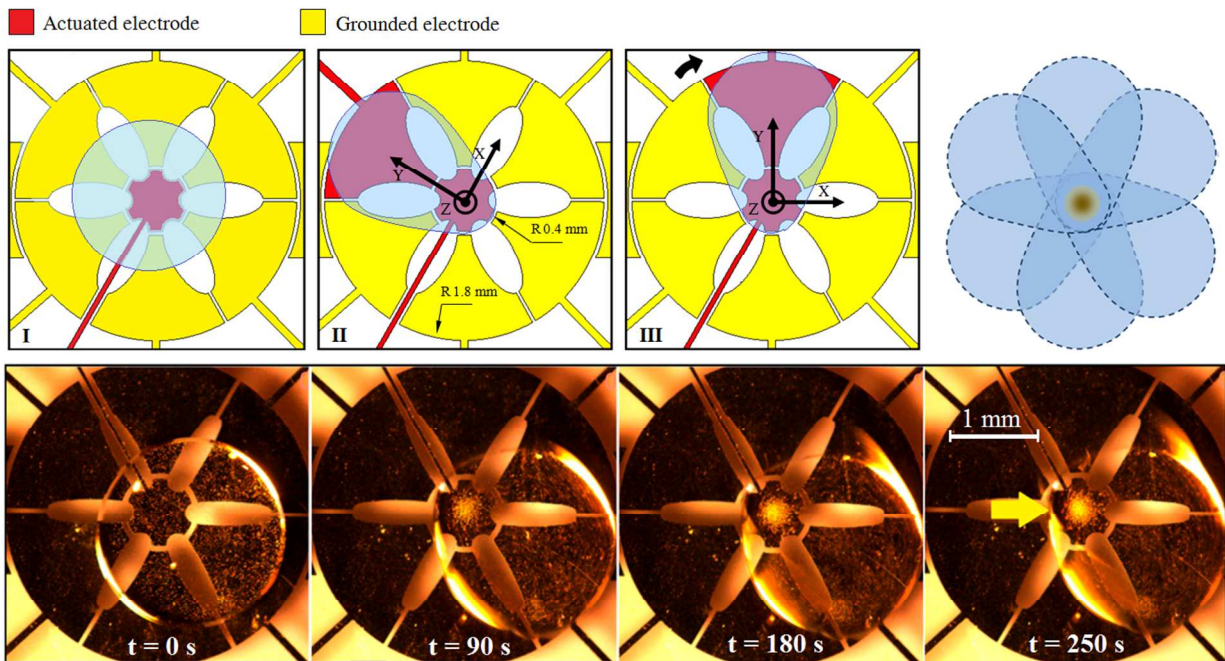
In the present study, the electrode configuration and actuation scheme are designed in a fashion to implement a gravity-based hydrodynamic particle separation method on digital microfluidic systems.

Gravity-driven hydrodynamic particle separation in digital microfluidic systems

Hojatollah Rezaei Nejad, Ehsan Samiei, Ali Ahmadi and Mina Hoorfar

University of British Columbia, 3333 University Way, Kelowna, BC, Canada V1V1V7

Corresponding author:

 Mina Hoorfar; Tel.: +12508078804; fax: +12508079850; mina.hoorfar@ubc.ca

Abstract

In the present study, a hydrodynamic particle manipulation method for digital microfluidic platforms is introduced to separate and concentrate non-buoyant particles in micro-droplets. The proposed method utilizes the combined effects of the gravitational forces and the fluid flow inside the droplet, and it depends only on the hydrodynamic properties of the system without the need of external electrical or magnetic modules. The desired hydrodynamic effect is created by manipulating the droplet in a controlled fashion on a circular pattern of electrodes using the electrowetting-on-dielectric technique. Two successful electrode designs (Star Design and Square Design) are presented. To investigate the feasibility of the proposed particle separation technique, suspensions of silica and polystyrene beads are tested. The fabricated devices successfully focus the non-buoyant silica beads of 1µm and 5µm and polystyrene beads of 15µm in a region on the central electrode; whereas the focusing behavior is not observed for the polystyrene beads of 5µm. A capturing efficiency of 86% and 94% are achieved for the 5-µm silica particles and 15-µm polystyrene particles, respectively. A parametric study is conducted to investigate the dependency of the focusing regimes to the particle size and density, the droplet size and the electrode geometry, and the actuation scheme. To understand the focusing mechanism, the fluid flow inside the droplet is simulated numerically, and the observed time scales are verified through analytical calculations. Finally, the application of the current particle focusing technique is illustrated for detection of the presence of a low concentration of DNA (18 µg/mL).

1. Introduction

Microfluidic devices have gained significant attention over conventional biochemical laboratory equipment mainly due to their small dimensions. These devices use small amounts of samples and reagents, and provide a large surface to volume ratio, resulting in reduced procedural costs, shorter reaction times and higher precision [1, 2]. Fluidic operations on these devices are typically performed using digital or continuous methods. Digital microfluidic (DMF) devices, which function based on handling discrete droplets, provide researchers with distinctive benefits (over the continuous microfluidic systems) including re-configurability and programmability [3, 4, 5]. A prodigious number of studies have been conducted to integrate biochemical laboratory processes into DMF platforms using basic droplet-based operations: merging, splitting, transport and dispensing [6, 7, 8]. However, a fundamental function in most of biochemical applications includes separation and concentration of particles and molecules [9, 10, 11, 12], which cannot be performed by these basic operators. Therefore, the development of particle separation techniques (for manipulating particles inside the droplets) is a crucial step in promoting DMF devices for numerous biological applications.

In the past decade, several techniques have been developed for particle manipulation in DMF platforms. These techniques include magnetic [13, 14], optic [15], electrophoretic [16, 17] and dielectrophoretic [18, 19, 20] methods. Although all these methods have successfully incorporated particle separation into DMF systems, each method is applicable to a specific range of droplet/particle physical properties, which limits the range of the applicability and scope of these techniques. For instance, electrophoretic and magnetic methods are effective in manipulating charged and magnetic particles, respectively. Although dielectrophoresis can be applied to a wider range of particles, it is more suitable for droplets with low conductivity. Methods such as optical tweezers eliminate the restriction on the conductivity of liquid. However, these methods require the use of external light sources. To extend the implementation of the DMF technology into a wider range of applications, it is important to develop alternative particle-focusing techniques which are not restricted by droplet/particle electromagnetic properties, and do not require additional external modules.

In the present study, a hydrodynamic-based particle manipulation method for DMF platforms is developed to concentrate and collect non-buoyant particles (of different sizes) in the droplets. The proposed methodology utilizes the combined gravitational and inertial effects inside the droplet, and it strongly depends on the hydrodynamic properties of the system without the need of external modules. In essence, the desired hydrodynamic effect is created by manipulating the droplet in a controlled fashion on a circular pattern of electrodes using the electrowetting-on-dielectric (EWOD) technique [21].

The article is organized as follows: Theory Section provides the theoretical background, and the Methodology Section introduces the experimental setup, fabrication procedure, numerical simulation and image processing algorithm. In the Results and Discussion Section, the results of

the proposed methodology are presented and discussed for suspensions of silica and polystyrene beads. To understand the focusing mechanism, the fluid flow inside the droplet is simulated numerically, and the observed time scales are verified through analytical calculations. A systematic study has been performed and the dependency of the focusing regimes to the particle size, the droplet/electrode size ratio, the electrode geometry, and the actuation scheme are investigated. Finally, three possible applications of the current technique are illustrated, including the detection of a low concentration DNA in the sample. The Conclusion Section describes the conclusions drawn from the present work.

2. Theory

Hydrodynamic forces have been used for manipulating particles in microfluidic systems for applications such as particle focusing and separation [22, 23]. The equation of motion of particles in the vector form can be formulated as [24]

$$m_p \frac{d\mathbf{u}_p}{dt} = \mathbf{F}_s + \mathbf{F}_B, \tag{1}$$

where m_p is the particle mass, $\mathbf{u}_p$ is the particle velocity, $\mathbf{F}_s$ is the surface force on the particle due to pressure and shear stresses imposed by the continuous phase, and $\mathbf{F}_B$ is the body force acting on the particle. In microfluidic applications, drag ($\mathbf{F}_D$) and lift ($\mathbf{F}_L$) forces are the main surface forces acting on the particle as [22, 23]

$$\mathbf{F}_s = \mathbf{F}_D + \mathbf{F}_L. \tag{2}$$

In the absence of electromagnetic effects, the main body forces acting on the particle are the gravitational ($\mathbf{F}_g$) and buoyancy forces ($\mathbf{F}_b$). Therefore, the equation of motion of the particle, Equation (1), can be written as

$$m_p \frac{d\mathbf{u}_p}{dt} = \mathbf{F}_D + \mathbf{F}_L + \mathbf{F}_g + \mathbf{F}_b. \tag{3}$$

The Reynolds number is one of the most important parameters in determining the magnitude of the forces in Equation (3) [22, 23], which is defined as

$$Re = \frac{\rho_f u_f L}{\mu_f}, \tag{4}$$

where ρ_f, μ_f and u_f are the fluid density, viscosity and velocity, respectively, and L is the characteristic length. Although the lift force plays an important role in inertial focusing of particles in microfluidic systems, it has been shown that it is only significant for intermediate and high Reynolds numbers ($\sim Re > 1$) [22, 23]. For the range of velocities and system dimensions used in this study, Reynolds number is smaller than one. Therefore, the equation of motion in the direction of gravity (z-direction) can be simplified to

$$m_p \frac{dw_p}{dt} = F_g - F_b - F_{Dz},\tag{5}$$

where w_p is the z-component of the particle velocity, and F_{Dz} is the Stoke's drag force (which is a good approximation for $Re < 1$) in the z-direction defined as

$$F_{Dz} = 3\pi\mu_f d_p(w_p - w_f).\tag{6}$$

In Equation (6), d_p is the particle diameter, w_f is the z-component of the fluid velocity. Due to the planar structure of digital microfluidic systems, the z-component of velocity, w_f, can be assumed to be zero inside the droplet in the regions which are not in the vicinity of the droplet-filler interface [25]. The body forces in Equation (5) can be expressed as

$$F_g = \rho_p V g\tag{7}$$

and

$$F_b = \rho_f V g.\tag{8}$$

where V is the volume of the particle. Integration of Equation (5) with the assumption of a zero initial velocity for a spherical particle leads to the following expression for the vertical velocity of the particle:

$$w_p(t) = w_\infty\left(1 - e^{-t/\tau}\right),\tag{9}$$

where

$$w_\infty = \frac{g(\rho_p - \rho_f)d_p^2}{18\mu_f},\tag{10}$$

and

$$\tau = \frac{\rho_p d_p^2}{18\mu_f}.\tag{11}$$

In the above relations, w_∞ is the terminal sedimentation velocity in the z-direction, and τ is a time constant related to motion of the particles in the fluid, which represents the time required for a quiescent particle to reach the local velocity of the fluid in the vertical direction. These time scales and velocities must be considered in the design of the DMF system to achieve the desired hydrodynamic separation regimes.

3. Methodology

3.1 Experimental procedure

The experimental setup used for this study is depicted in Fig. S1. The setup consists of a closed DMF device (consisting of the top and bottom plates sandwiching the droplet) connected to an AC voltage supply unit. The required voltage for droplet actuation is supplied by a signal function generator (Tektronix AFG3021B0) connected in series with an amplifier (TREK PZD700) to magnify the generated signal. An Apo-zoom microscope (Leica Z6 APO) is used to monitor the experiment which is equipped with a high speed camera. The experiments are performed on three different designs of an array of electrodes shown in Fig. S2a (Star design), Fig. S2b (Circular design) and Fig. S2c (Square design). Each array includes a central electrode surrounded by six electrodes for the Star design and eight electrodes for the Circle and Square designs. In all designs, each of the electrodes is separately addressable. A droplet containing the particles is dispensed on the center of the design, and then sandwiched between the top and bottom plates, kept at a constant gap height of 320 μm using a set of spacers. The central electrode is turned on and kept activated throughout the experiment; while the surrounding electrodes are sequentially activated for 125 ms. One surrounding electrode is actuated at a time for the Star design whereas two surrounding electrodes are actuated simultaneously for the Circular and Square designs (to preserve the egg-shape of the droplet during the rotation). The actuation scheme used for each design is depicted in Fig. S2. An AC voltage with the amplitude of 100 V_{rms} and frequency of 1 kHz is used for actuation. As it is shown in Fig. S2, the droplet is elongated between the central and the actuated surrounding electrode as the voltages are applied. Under this actuation scheme, the droplet spins around the center of the central electrode after actuating each surrounding electrode.

The samples contain DI water (with a measured conductivity of 2 μS/cm [26]) and silica (Si) or polystyrene (PS) particles. The density of PS and Si particle are 1.06 and 2.5 gr/cm^3 , respectively. The experiments are performed on of the silica particles with the diameters of 1μm and 5μm (namely Si-1 and Si-5) and PS particles of 5μm and 15μm (namely PS-5 and PS-15). The conductivity of the final liquid sample for silica and polystyrene beads are 35 μS/cm and 7 μS/cm, respectively. All samples are prepared with the same volume fraction (0.1 v/v%).

3.2 Device fabrication

A copper coated glass substrate (with a copper layer thickness of 50 nm) is used for the bottom plate. The electrodes are patterned on the substrate by standard photolithography. The procedure is as follows: a layer of the S1805 photoresist (MicroChem Corp.) is coated on the copper at 2000 rpm for 60 s, and soft baked for 2 min at 95 ℃. It is then exposed to UV light through a mask containing the design. Afterwards, the substrate is immersed in a developer for 30 s, and then etched in the copper etchant for 30 s. To create dielectric layer on the electrodes, Parylene C with a thickness of 4 μm is deposited on the patterned electrodes through a CVD process. In the next step, a Teflon AF 1600 (DuPont) solution with a 3% w/w concentration is coated on the dielectric layer at the speed of 2500 rpm for 60 s. The chip is then baked at 95 ℃ for 2 hours. An

ITO glass slide (SiO$_2$ passivated, $R_s = 4 - 8\,\Omega$) covered by a layer of Teflon AF (with the same thickness as the bottom plate) is used for the top plate.

3.3 Numerical simulation

For the simulation of the fluid flow inside the droplet, the coordinate system is placed on the droplet to achieve a steady-state regime. As shown in Fig. S3, an elongated droplet with the volume of 2 μL, covering the central and a surrounding electrode, is simulated. Due to the low concentration of the particles, the fluid is assumed to be Newtonian with water properties. Navier-Stokes and continuity equations [27] are solved to obtain the velocity and pressure fields inside the droplet. Due to the symmetry of the flow with respect to the central plane, half of the flow domain is simulated. An unstructured hexahedral grid is generated in the simulation domain using ANSYS® Workbench 14.5. The total number of 523484 mesh elements is chosen after the mesh-independency study, considering the fluid velocity as the evaluation criterion. The commercial Computational Fluid Dynamic (CFD) software package FLUENT 14.5 (ANSYS Inc.), which is a finite volume-based solver [28], is used to solve the fluid flow equations. A second order upwind method is used for discretization of the momentum equations, and a standard SIMPLE scheme is adopted for pressure-momentum coupling [28]. The convergence criterion for the momentum and continuity equations is 10^{-6}. The zero-shear wall boundary condition (slip wall with the zero shear stress at the wall) is used for the sides of the droplet (which is a suitable model for the boundary condition of a gas-liquid interface). A rotational velocity boundary condition with the rate of 8.4 rad/s (see Fig. S3) is used for the bottom plane. A no-slip boundary condition is used on the solid surface [29], and a symmetric boundary condition is used for the top plane.

3.4 Image processing

An image processing technique is used to count the number of particles in the droplet. For this purpose, top-view images of the droplet are acquired with high resolution (2592 pixels × 1944 pixels). The background is removed, and the noise is minimized by increasing the contrast in the image. A filter with one-intensity threshold is then applied to the images. In each image, pixels with the intensity value less than the threshold and more than zero (i.e., the intensity of the background) are considered as the first layer of the particles. For the intensity values larger than the threshold, the pixels are considered as the second layer of the particles. In the next step, the image is divided into smaller sub-regions, and the number of particles in each sub-region is calculated (Number of particles in an area = (Number of pixels in the 1st layer + 2 × Number of pixels in 2nd layer) / (pixel size of the particle)). The filter threshold and the average pixels size of a particle are calculated through a calibration process explained in Supporting Information (SI).

4. Results and discussion

In this section, the particle-focusing behavior is studied using the proposed chip configurations (Fig. S2). As described in Section 3.1, two actuation schemes and therefore two distinct droplet motion regimes are studied: 1) the droplet is continuously spun about the axis of rotation by constant actuation of the central electrode and actuation of all surrounding electrodes; and 2) the droplet moves in a pendulum motion by constant actuation of the central electrode and actuating three of the surrounding electrodes (as shown in Fig. S4). In the following sections, the feasibility of the proposed methodology is highlighted. In Section 4.1, the capability of the proposed method in focusing particles of different sizes (Si-1, Si-5 and PS-5) are tested on the Star design. In Section 4.2, the physics involved in the proposed focusing mechanism is explained. In Section 4.3, the particle (Si-5 and PS-15) focusing behavior for different geometries of the central electrode (Star, Circle and Square designs) are illustrated. In Section 4.4, the effects of the droplet volume, the particle size and density on the particle (Si-5 and PS-15) focusing efficiency for two electrode geometries (Star and Square designs) are characterized. Finally, in Section 4.5, three possible applications of the proposed technique (droplet purifications, particle-particle interaction, and DNA detection) are explored.

4.1 Proof of concept

To investigate the feasibility of the proposed particle-focusing technique, suspensions of Si-1, Si-5 and PS-5 are tested using the Star design. For all cases, the droplet size of $V_d = 1.2$ μL is chosen. As it is shown in Fig. 1a and 1b, the fabricated device successfully focuses the Si-1 and Si-5 beads in the center of the central electrode. Interestingly, the focusing behavior is not observed for PS-5 beads (Fig. 1c). This shows that the density difference between the particles and surrounding liquid (and the resulting particle sedimentation) plays a crucial role in focusing the particles. The comparison between the size of the focused regions observed for the cases of Si-1 and Si-5 particles shows that a larger region is covered for the Si-5 particles (which have a higher diameter) despite the fact that both solutions have the same volume fraction of the particles (0.1 v/v%). This shows that the efficiency of particle focusing is also a function of the particles diameter.

To investigate the focusing behavior in more depth, the effects of the actuation scheme is studied. To achieve a new actuation scheme only three adjacent surrounding electrodes are actuated periodically to create a pendulum motion. As it can be seen in Fig. 4Sa, the shape of the focused region changes to a crescent as the actuation scheme is changed to pendulum motion. The observed shape seems to be related to the motion of the three-phase contact line of the droplet around the central electrode. The three-phase contact line (the portion that is in contact with the central electrode) moves in a semi-circle shape (see the schematic in Fig. S4a), which is very similar to the crescent shape of the focusing region. This shows that the location of the

8

interface on the central electrode can affect the focusing behavior significantly. To investigate this effect more in depth, experiments were carried out for two different droplet sizes: 0.8μL (Fig. 4Sb) and 1.2 μL (Fig. 4Sc). The small droplet is chosen in a way that there is no (or minimum) overlap between the droplet and the center point of the central electrode. As it can be seen in Fig. 4Sb, no focusing behavior is observed for the smaller droplet; while successful focusing is achieved for the larger droplet. Therefore, the droplet volume should be chosen in a way to cover the central electrode. This will create a low velocity region (dead zone) above the central electrode, and hence, the particles that sediment in the region will stay there. In other words, particle focusing happens only when the central region of the central electrode is covered with the droplet.

4.2 Simulation and analytical study

To gain a better insight into the focusing mechanism, the fluid flow inside the droplet is simulated using the method described in Section 3.3. As explained before, the coordinate system is moving with the droplet. Thus, to satisfy the no-slip boundary condition, the fluid at the bottom plate (at z = -150 μm) is moving with the same velocity as the relative velocity of the plate [25]. Figure 2 shows flow streamlines in different planes inside the droplet. As it is expected, all the streamlines are closed, and due to the dominant effect of the drag force compared to that of the lateral lift force, buoyant particles of the small sizes are carried along these streamlines. Therefore, if the gravitational force on the particles is insignificant, particles always flow in the bulk of liquid without focusing into any specific region. This confirms the results shown in Fig. 1c for the PS-5 particles. On the other hand, denser particles (compared to the liquid) sediment due to the gravitational force, and gradually move from one streamline to another with a lower elevation. This continues until the particles sediment into one of the two regions on the bottom plate: Zone 1 (referred to as dead zone) or Zone 2. The dead zone is shown as a yellow region in Fig. 2c at z = -145 μm with closed planar stream lines. Zone 2 is shown with the orange color in Fig. 2c with planar and three dimensional (3D) streamlines around the dead zone. In the central region of Zone 2 (away from the side boundary) the streamlines are planar. However, in regions very close to the triple-phase contact line, there is an out of plane motion, and the streamlines continue vertically (the gray parts of the streamlines in Fig. 2c) to other planes with higher elevations. This is confirmed by considering the z-component of the velocity shown in Fig. 2c. If the particles sediment into Zone 2, they will be lifted to a higher elevation as they approach the triple-phase contact line due to their z-component of velocity. These lifted particles sediment to streamlines in lower planes, and get closer and closer to the region above the dead zone, and ultimately sediment into this region. The particles, which sediment into the dead zone, will be trapped, increasing the concentration of the particles in this zone. As a result, all the non-buoyant particles are gradually trapped and focused in the dead zone on the bottom plate.

9

To verify the validity of the above explanation and compare the observed time scales, a theoretical analysis of the particle motion is presented here. For the present geometry, the response time calculated from Equation (11) for the Si-1 and Si-5 particles are $\tau = 0.139 \ \mu s$ and $3.47 \ \mu s$, respectively. The calculated response time is the time needed for the z-component of the particle velocity (w_p) to approximately become w_∞ (the terminal sedimentation velocity in the z-direction). Therefore, with a good approximation, it can be assumed that the particles sediment with their terminal velocities. The terminal sedimentation velocity for Si-1 and Si-5 particles, obtained from Equation (9), are $w_\infty = 0.817 \ \mu m/s$ and $20.4 \ \mu m/s$, respectively. Based on the angular velocity of the droplet and dimensions of the system, the average horizontal velocity (in the $x - y$ plane) for a particle moving in the middle plane above the dead zone is $0.5 \ mm/s$ (which is found from the results of the numerical simulation). On the other hand, based on the value of w_∞ and the dead zone size, the 1-μm and 5-μm silica particles (Si-1 and Si-5) will sediment (on average) by $1 \ \mu m$ and $25 \ \mu m$ per one round of rotation, respectively, during their travel over the dead zone in the middle plane. Therefore, the particles traveling above the dead zone are expected to sediment into the dead zone after a finite number of rotations. Although these calculations are based on the average values, and the sedimentation length is different at different planes, they are in agreement with the fact that the larger particles focus with a faster rate (see Fig. 1 and Fig. 4). Thus, the proposed hydrodynamic particle separation method utilizes the combined effects of the gravitational forces and the fluid flow inside the droplet, and it strongly depends on the hydrodynamic properties of the system.

4.3 Effects of the geometry

As discussed in the previous section, particle focusing using the proposed technique depends on the shape of the dead zone, which depends on the geometry of the central electrode. Therefore, it is expected that the geometrical configuration of the device plays an important role in the effectiveness of the proposed method. To study the effects of the geometry of the central electrode, two other geometries, i.e., Square and Circle designs, are studied in addition to the Star design (see Fig. S2). These two designs have a similar size surface area of $1.44 \ mm^2$ which is larger than that of the star design (i.e., $0.4 \ mm^2$). Solutions of Si-5 and PS-15 with the volume fraction of 0.1% (vt/vt) are used for the experiments. Fig. 3 shows the initial condition (the left image for each case) and the condition at $t = 250 \ s$ at which the particles are focused (the right image for each case). As shown in Figs. 3a and 3b, the focusing efficiency of the Star design is higher for Si-5 compared to the PS-15 particles.

Although the Circle design has a larger central electrode in comparison with the Star design, particle focusing is not observed for this design, see Fig. 3c and 3d. This shows that presence of sharp corners for the central electrode design is essential to observe focusing behavior (e.g. Square and Star design).

Figures 3e and 3f show the results of the Square design with PS-15 and Si-5, respectively. It is observed that for both cases of PS-15 and Si-5, the particles are concentrated on the central electrode. The area of the central electrode in this design is equal to that of the Circle design. However, the focusing behavior for the Square design is very different due its square shape: while the droplet spins around the central electrode, the interface pins at the corners of the square, and hence the majority of the streamlines pass over the central electrode. Therefore, particles have a high chance to sediment into this region. The difference between PS-15 and Si-5 in the focused region for this design is that the PS-15 particles form a doughnut shape while the Si-5 particles form a circular shape.

4.4 Parametric study

4.4.1 Particle density and size

In Sections 4.1 and 4.3, it was shown that particle-focusing behavior depends on the size and density of the particles, the droplet size, and the geometry of the central electrode. In this section, the effects of these parameters will be studied in depth. Since no particle-focusing behavior was observed for the Circle design, only Star and Square designs are chosen for this part of the study. To consider the size and the density of the particles, Si-1, Si-5, PS-5 and PS-15 are used for the experiments.

The dynamic behavior of particle focusing is studied by measuring the ratio of (n_c/n_t), where n_c is the number of the trapped particles on the central electrode and n_t is the total number of particles in the droplet. Figures 4a and 4b show n_c/n_t versus time for the Star and Square designs, respectively. The difference in the initial number of particles in Fig. 4a and 4b is due to the difference between the surface area of the central electrode for the Star (0.4 mm^2) and Square designs (1.44 mm^2).

In the case of the Star design (Fig. 4a), all the curves are ascending (showing the increase in the number of the focused particles over time) except for PS-5, which is almost plateau over the entire process. This behavior of the PS5 particles is observed as they have a low density and diameter (compared to PS15), which were previously shown to be the key parameters for successful particle focusing. For other particles, the number of particles trapped on the central electrode increases continuously. However, the slope of the curves decreases over time, which shows that there is a saturation limit for the focusing behavior. This saturation is expected to happen when all the particles are trapped.

Figure 4b (the Square design) illustrates that the number of the focused particles has an ascending trend, except for PS-5 that the curve is descending, which means over time, PS-5 particles move away from the central electrode. Also, a capturing efficiency (n_c/n_t) as high as

11

96% was achieved for focusing of PS-15 in the Square design, which shows a significant increase over the Star design producing the capture efficiency of 25% for PS-15.

The comparison between particles of the same size (Si-5 and PS-5) and particles of the same density ((PS-5 and PS-15) or (Si-1 and Si-5)) in Fig.4 shows that both particle density and size are important in the focusing behavior. In essence, by increasing the particle density or size, the focusing behavior can be enhanced.

4.4.2 Droplet volume

As shown in Section 4.1, in order to have successful particle focusing, the droplet size should be large enough to cover the central electrode. However, one needs to study which droplet volume could result in the highest focusing efficiency. Therefore, the effects of the droplet size is studied by performing the experiments with a range of droplet sizes from 0.9 µL to 1.9 µL containing Si-5 or PS-15 particles (as particles of high and low densities that have shown higher focusing efficiency for both Star and Square designs (see Fig. 4)). Three parameters are compared in this part based on: 1) the size and the shape of the focused region, 2) the ratio of the maximum to the initial concentration of the particles in the focused region, and 3) the ratio of the number of the focused particles over the total number of the particles in the droplet (n_c/n_t). The samples were dispensed on the chip using a calibrated pipette with the range of volumes starting from 0.9 µL to 1.9 µL with an increment of 0.1 µL. To ensure that the sizes of the droplets dispensed using the pipette are accurate, the droplet sizes were measured by image processing. The surface area of the droplet was accurately measured using the ImageJ software package, and the measured surface area was multiplied by the gap height between the top and bottom plates to calculate the droplet volume. Thus, the data reported here are based on the determined values from image processing. All the results presented here are measured at the time of $t = 250$ s.

Figures 5a and 5b show the size of the focused region for the PS-15 and Si-5 particles, respectively. As explained before, the Si-5 particles that are focused on the central electrode for both the Star and Square designs form a circle filled completely with particles (shown in Figs. 3b and 3f), which is quantified by considering the diameter of the circle (D_o). For the PS-15 particles, on the other hand, the focusing region is more in the form of a doughnut shape on the Square design (shown in Fig. 3e), and hence, both inner (D_i) and outer (D_o) diameters of the focused region are measured. However, for a large volume of the droplet (droplet volumes larger than 1.6 µL) the shape of the focus region changes to a circle filled with particles (that is why in Fig. 5a just the outer diameter of the focusing region is reported for droplet volumes bigger than 1.6 µL). It should be noted that for any droplet volumes for which the focusing behavior is not observed, no data is shown in the graphs.

In the case of the Star design, the diameter of the focused region (D_o) (for both Si-5 and PS-15) does not change as the droplet volume changes. This observation suggests that the size of the focused region is more defined by the electrode size than the droplet volume. On the other hand, for the Square design, the inner (D_i) and outer (D_o) diameters linearly increase as the volume of the droplet increases, but interestingly the thickness of the focusing region ($D_o - D_i$) remains nearly constant (see Fig. 5a and Fig. 5b).

Most of the particles that are gathered on the central electrode are trapped in a circular pattern (named the focusing region). The concentration of the particle (defined as the number of the particles divided by the area of the interest) in that region is much higher than other parts of the droplet. Figures 5c and 5d show the concentration of the particles in the focusing region (C_m) which is normalized based on the initial concentration of the particles in the droplet (C_0) for different droplet volumes. Due to the slight difference between the numbers of the particles in each dispensed droplet, the initial concentration of the particles for all tested droplets is measured using the image processing technique. As it can be seen in Figs. 5c and 5d, the curves have an optimum point. For the PS-15 particle, the maximum concentrations observed for both the Star and Square designs happens for volumes between 1.2 μL to 1.3 μL, respectively, and a higher concentration ratio was achieved using the Square design ($C_m/C_0 \approx 4.5$). In general, a similar trend for both electrode designs has been observed for the PS-15 particles. Also, for both cases the trend is sensitive to the droplet volume. On the other hand, the particle-focusing behavior for Si-5 is very different for the two electrode designs. For the Star design, the concentration in the focused region (C_m) is very sensitive to the droplet size and has a relatively sharp peak at the droplet volume around 1.1 μL at which the concentration of the particles in the focusing region is more than 12 times of the initial concentration. However, for the Square design, the concentration in the focused region (C_m) does not change significantly as the droplet volume varies. This is because of the fact that the surface area of the Square design is 3.6 times larger than that of the Star design, and hence, the particles can spread in a much larger area.

Figures 5e and 5f show n_c/n_t (the ratio of the number of the focused particles over the total number of the particles in the droplet) versus the droplet volume for PS-15 and Si-5, respectively. However, the peak value for each case happens at different droplet volumes: in the case of the Star design, the optimum volumes to achieve a high capturing efficiency are 1.1 μL and 1.2 μL for the Si-5 and PS-15 particles, respectively. For the Square design, the optimum volume is found to be 1.2 μL and 1.3 μL for the PS-15 and Si-5 particles respectively (see Fig. 5e and 5f). This suggests that the optimum volume is a function of the design geometry and the particle size/density. Based on Figs. 5e and 5f, the total number of the trapped particles using the Star design does not exceed 50% of the total number of the particles. This is primarily because of the small size of the central electrode in comparison to the total size of the system. However, as it can be observed in Figs. 5c and 5d, a high local concentration could be achieved using the Star design for Si-5. These results suggest the applicability of the Star design for particle focusing (high local concentration) rather than particle separation (total number of the trapped particles).

13

On the other hand, Figs. 5e and 5f show that using the Square design, particles can be effectively gathered (after 250s) up to 94% for PS-15 and 86% for Si-5, which makes the Square design suitable for separation applications.

4.5 Applications

So far, it is shown that the particle-focusing technique proposed in this paper can concentrate non-buoyant particles with a wide range of relative densities. The effects of the parameters such as the electrode geometry, the size and the density of the particles, and the droplet size were thoroughly studied on the focusing efficiency. Some possible applications for the proposed technique are discussed in the following subsections:

4.5.1 Concentrating particles

One possible application of the proposed technique is to increase the concentration of particles in a droplet on the chip. In this case, by spinning a mother droplet with a low concentration of particles, the particles can be focused on one side of the droplet. By using neighbor electrodes, the mother droplet can be split into two daughter droplets [30], in which one contains a higher concentration and the other with a low concentration of the particles. This scenario is shown in Fig. S5 where the initial mother droplet contains the Si-5 particles (Fig. S5a). The mother droplet is spun around the central electrode and when the desired concentration of the particles is achieved the spinning process is stopped (see Fig. S5b). The droplet is then split into two daughter droplets as shown in Figs. S5c and S5d. The final step is to move the daughter droplets to the other parts of the chip to use them in desired applications. This process is shown in Figs. S5e and S5f.

4.5.2 Particle-particle interaction

As discussed previously, the PS-5 particles cannot be focused using the proposed designs (see Figs. S6a and S6b for a 1.1- μL droplet). However, when a very small number of the PS-15 particles are added to the solution, the particle-focusing behavior will be very different. As shown in Figs. S6c and S6d, the PS-5 particles are focused on the central electrode and form a ring where the PS-15 particles surround the ring. The large particles possibly act as a filter and hold the smaller particles inside the ring. This shows that the focusing behavior of one type of particle (PS-5) makes it possible to detect the presence of another type of particle (PS-15) with a much lower concentration in the droplet. This potentially can be used to detect larger target cells, bacteria or particles without using a detector. In other words, one can add PS5 particles to the biological sample. If there are large size molecules inside the droplet, the focusing behavior will

14

be observed for the PS5 particles. Otherwise, the PS5 particles will not be focused, confirming the fact that there are no large particles in the sample.

4.5.3 DNA detection

In this section an application of the developed technique is presented for the detection of the presence of a low concentration of DNA. To illustrate the detection of DNA using the developed technique, a solution is prepared using the PS-15 particle sample (explained in the Experimental procedure section) by adding purified human saliva DNA[31]. The final solution has the DNA concentration of 18 µg/mL obtained using NanoDrop 2000 Spectrophotometer (Thermo Fisher Scientific, Inc.). The focusing test is performed for two different samples: with and without DNA. For this purpose, two droplets with an identical size (1.5 µL) are dispensed on the chip including a square-shape central electrode. As shown in Fig. S7, different focusing regimes are observed for the two solutions after 250 s. In essence, 83% of PS particles are focused on the central electrode in the absence of DNA in the solution (shown in Fig. S7a). However, for the sample with DNA no focusing behavior is observed and only 19% of the particles are on the central electrode region (shown in Fig. S7b). In fact, adding DNA to a buffer changes the viscosity of the buffer[32], and therefore, the observed difference in the focusing behavior of the PS particles can be attributed to the change in the viscosity of the solution. This change in the behavior of the particle focusing regime provides a powerful tool for the on-chip detection of a low concentration of DNA.

5. Conclusions

In the present study, a hydrodynamic-based particle focusing technique, which is independent of the electromagnetic properties of the particles/fluid, is proposed for DMF platforms. The technique uses cumulative effects of gravitational and hydrodynamic effects to focus the particles in the center of the design in a two-plate DMF platform. The physics of the phenomenon is studied both analytically and experimentally, and it is shown that by rotating a droplet containing micro-particles around the center point the particles can be focused on the central electrode. Moreover, the effects of the electrode geometry (Star, Square and Circle designs), the droplet actuation scheme, the particle size and density (polystyrene particles of 5 and 15 µm and silica particles of 1 and 5 µm), and the droplet volume on the focusing behavior are studied. It is shown that the Star and Square designs can successfully focuses the 1-µm and 5-µm silica particles and 15-µm polystyrene particle into the central region of the design on the bottom plate of the DMF platform. The Star design has shown to be very effective for creating a high concentration of the silica particles (12 times higher than the initial concentration). On the other hand, the Square design has shown to be very effective in capturing polystyrene and silica particles in the droplet. The capturing efficiencies of 94% and 86% are achieved for droplets

containing polystyrene and silica particles, respectively. It is observed that for larger particle sizes and densities the capture efficiency is higher. In addition, the capture efficiency is a function of the droplet size, showing an optimum value for the droplet volume which results in the highest efficiency. Finally, three possible applications (i.e. droplet purification, and particle-particle interaction, and DNA detection) are introduced for the proposed particle focusing method.

References

[1] J. Mok, M.N. Mindrinos, R.W. Davis, M. Javanmard, *PNAS*, 2014, 111, 2110.

[2] E.K. Sackmann, A.L. Fulton, D.J. Beebe, *Nature*, 2014, 250, doi: 10.1038/nature13118.

[3] M.J. Jebrail, M.S. Bartsch, K.D. Patel, *Lab Chip*, 2012, 12, 2452.

[4] B. Hadwen, G. R. Broder, D. Morganti, A. Jacobs, C. Brown, J. R. Hector, Y. Kubota, H. Morgan, *Lab Chip*, 2012, 12, 3305.

[5] A. Ahmadi, K.D. Devlin, H. Najjaran, J.F. Holzman, M. Hoorfar, *Lab Chip*, 2010, 10, 1429.

[6] R. Sista , Z. Hua, P. Thwar, A. Sudarsan, V. Srinivasan, A. Eckhardt, M. Pollack, V. Pamula, *Lab Chip*, 2008, 8, 2091.

[7] I. Barbulovic-Nad, H. Yang, P.S. Park, A.R.Wheeler, *Lab Chip*, 2008, 8, 519.

[8] G.J. Shah, H. Ding, S. Sadeghi, S. Chen, C.J. Kim, R.M. van Dam, *Lab Chip*, 2013, 13: 2785.

[9] J. M. Martel, M. Toner, *Scientific Reports*, 2013, 3, 3340.

[10] X. Xuan, J. Zhu, C. Church, *Microfluid. Nanofluid.*, 2010, 9: 1.

[11] A.A. Bhagat, H. Bow, H.W. Hou, S.J. Tan, J. Han, C.T. Lim CT, *Med. Biol. Eng. Comp.*, 2010, 48, 999.

[12] H. Amini, E. Sollier, W.M. Weaver, D. Di Carlo, *PNAS*, 2012, 109, 11593.

[13] R.S. Sista, A.E. Eckhardt, V. Srinivasan, M.G. Pollack, S. Palanki, V.K. Pamula, *Lab Chip*, 2008b, 8, 2188.

[14] Y. Wang, Y. Zhao, S.K. Cho, *J. Micromech. Microeng.*, 2007, 17, 2148.

[15] G.J. Shah, A.T. Ohta, E.P.-Y. Chiou, M.C. Wu, C.J. Kim, *Lab Chip*, 2009, 9, 1732.

[16] S.K. Cho, C.J. Kim, *Proceedings IEEE Sixteenth Annual International Conference on Micro Electro Mechanical System*, 2003, 686–689.

[17] S.K. Cho, Y. Zhao, C.J. Kim, *Lab Chip*, 2007, 7, 490.

[18] H. Rezaei Nejad, O.Z. Chowdhury, M.D. Buat, M. Hoorfar, *Lab Chip*, 2013, 13, 1823.

[19] H. Rezaei Nejad, M. Hoorfar, Microfluidics and Nanofluidics, 2014, DOI:10.1007/s10404-014-1446-3.

[20] S.K. Fan, P.W. Huang, T.T. Wang, Y.H. Peng, *Lab Chip*, 2008, 8, 1325.

[21] F. Mugele, J.C. Baret, *J. Phys.: Condens. Matter*, 2005, 17, 705.

[22] H. Amini, W. Lee, D. Di Carlo, *Lab Chip*, 2014, DOI: 10.1039/C4LC00128A.

[23] J.M. Martel, M. Toner, *Annu. Rev. Biomed. Eng.*, 2014, 16, 371.

[24] E. Loth, A.J. Dorgan, *Environ. Fluid. Mech.*, 2009, 9, 187.

[25] A. Ahmadi, H. Najjaran, J.F. Holzman, M. Hoorfar, *J. Micromech. Microeng.*, 2009, 19, 065003.

[26] M.H. Banna , H. Najjaran, R. Sadiq, S. A. Imran, M. J. Rodriguez, M. Hoorfar, *Sensors and Actuators B: Chemical*. 2014, 193, 434.

[27] F.M. White, Viscous fluid flow, McGraw-Hill, 2005.

[28] J.D. Anderson, Computational fluid dynamics, McGraw-Hill, 1995.

[29] A. Ahmadi, J.F. Holzman, H. Najjaran, M. Hoorfar, *Microfluid. Nanofluid.*, 2010, 10, 1019.

[30] E. Samiei and M. Hoorfar, J. Micromech. Microeng., 2015, 25, 055008.

[31] Ovee Chowdhury, H. Rezaei Nejad, S. Gill, M. Hoorfar, "DNA Purification On Digital Microfluidics Platforms", *Proceedings of CSME International Congress*, June 1-4, 2014, Toronto, Ontario, Canada.

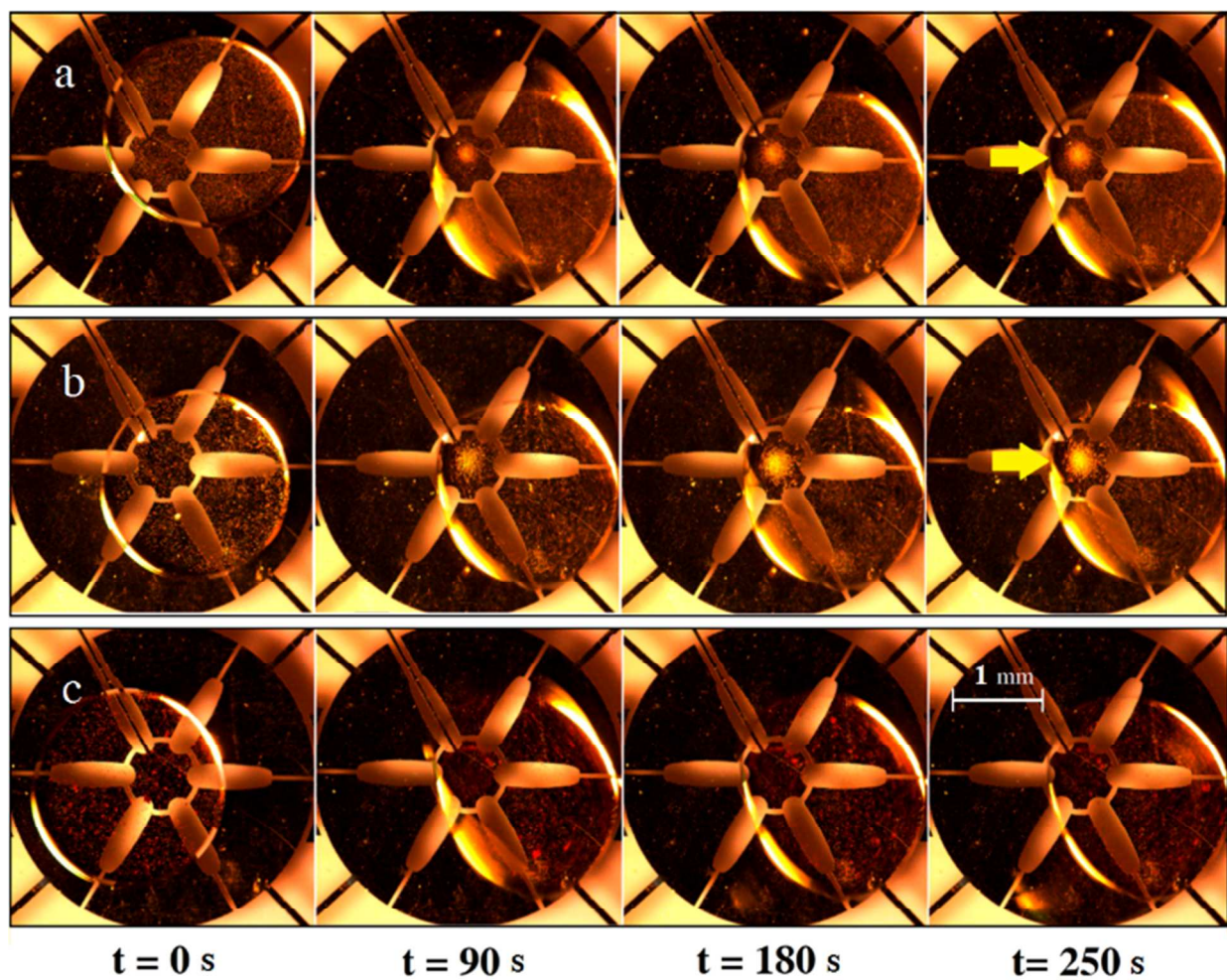[32] Sung Sik Lee, Kyu Hyun, Seong Jae Lee, Ju Min Kim, *Nature communications,* 2013, 4.

18

Fig 1 Particle focusing using the Star design for a) Si-1 (1 μm silica particles), b) Si-5 (5 μm silica particles), and c) PS-5 (5 μm polystyrene particles). For all cases the droplet size is $V_d = 1.2$ μL.
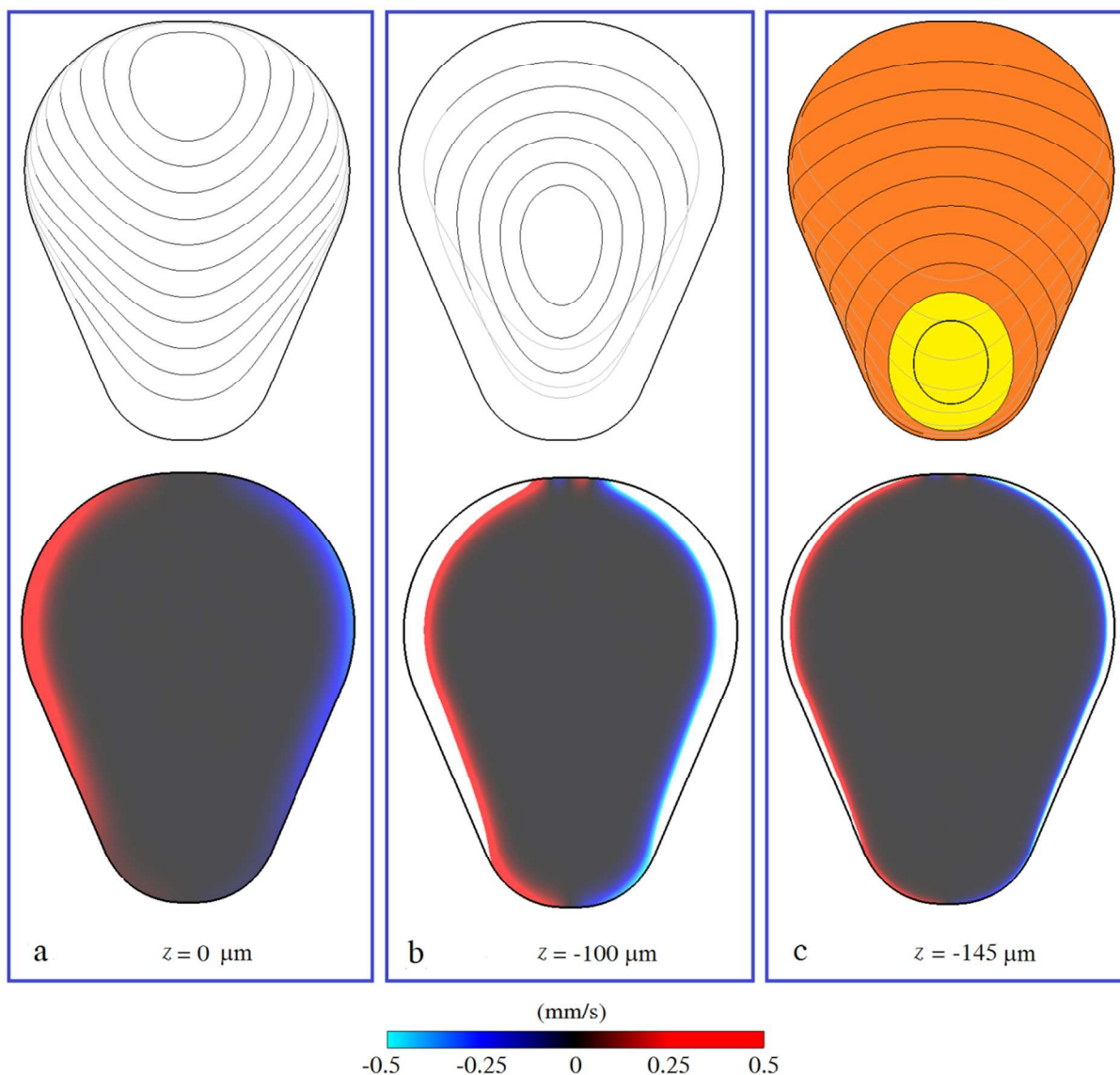
Fig 2 Streamlines and contours of the *z*-component of the fluid velocity in different planes (*z* = 0 (middle plane), *z* = -100 µm and *z* = -145 µm). The black part of the streamlines in the top-row images is in the pertinent plane while the gray part is out of the plane of motion. The range of the velocity contour shown in the bottom-row images is limited between -0.5 mm/s and 0.5 mm/s, and the regions with the greater magnitudes of the *z*-component of the velocity are shown in white. The maximum magnitude of the *z*-component of the velocity is found to be 6.5 mm/s, which happens at the gas-liquid interface (with the zero-shear wall boundary condition). The region shown in yellow at *z* = -145 µm (the bottom plate) is the dead zone, and the rest is Zone 2 described in the manuscript.
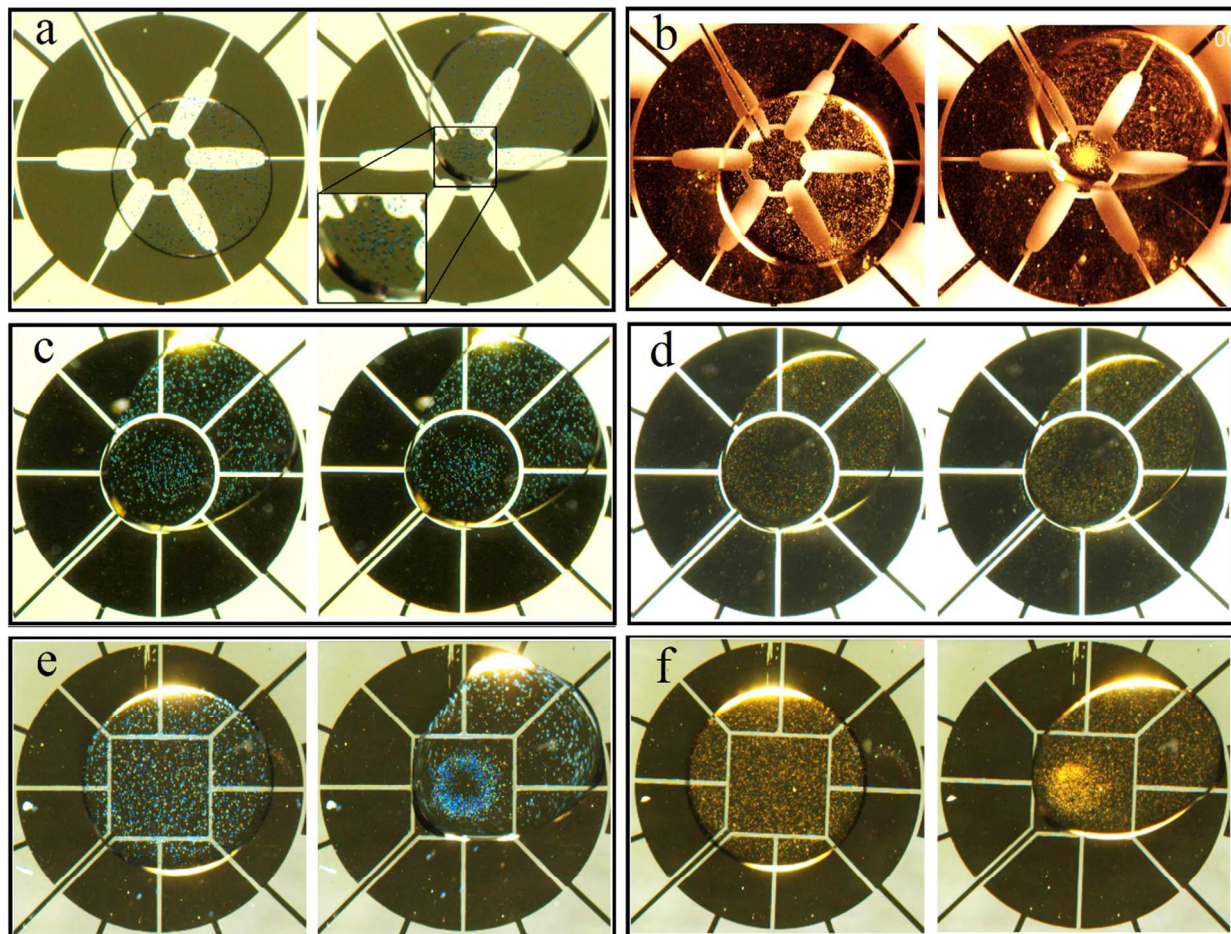
Fig 3 Particle-focusing using the three configurations of the central electrode including Star, Circle and Square with PS-15 and Si-5 particles. a) Star design and PS-15, b) Star design and Si-5, c) Circle design and PS-15, d) Circle design and Si-5, e) Square design and PS-15 and f) Square design and Si-5.
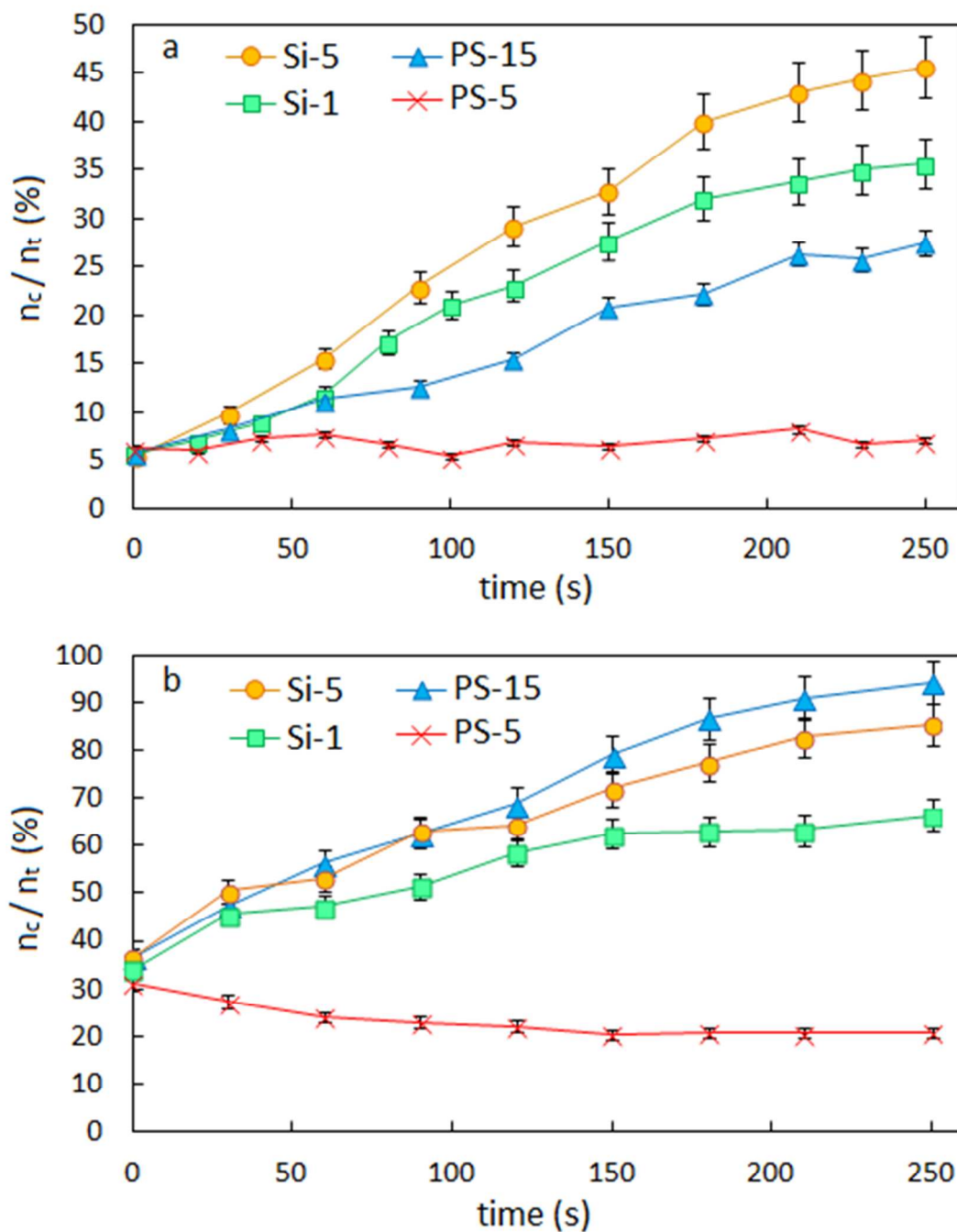
Fig 4 The percentage of the number of captured particles on the central electrode over time for the a) Star design, and b) Square design. Here n_c is the number of the trapped particles on the central electrode and n_t is the total number of particles in the droplet. For all cases the droplet volume is $V_d = 1.2 \pm 0.1 \, \mu L$.
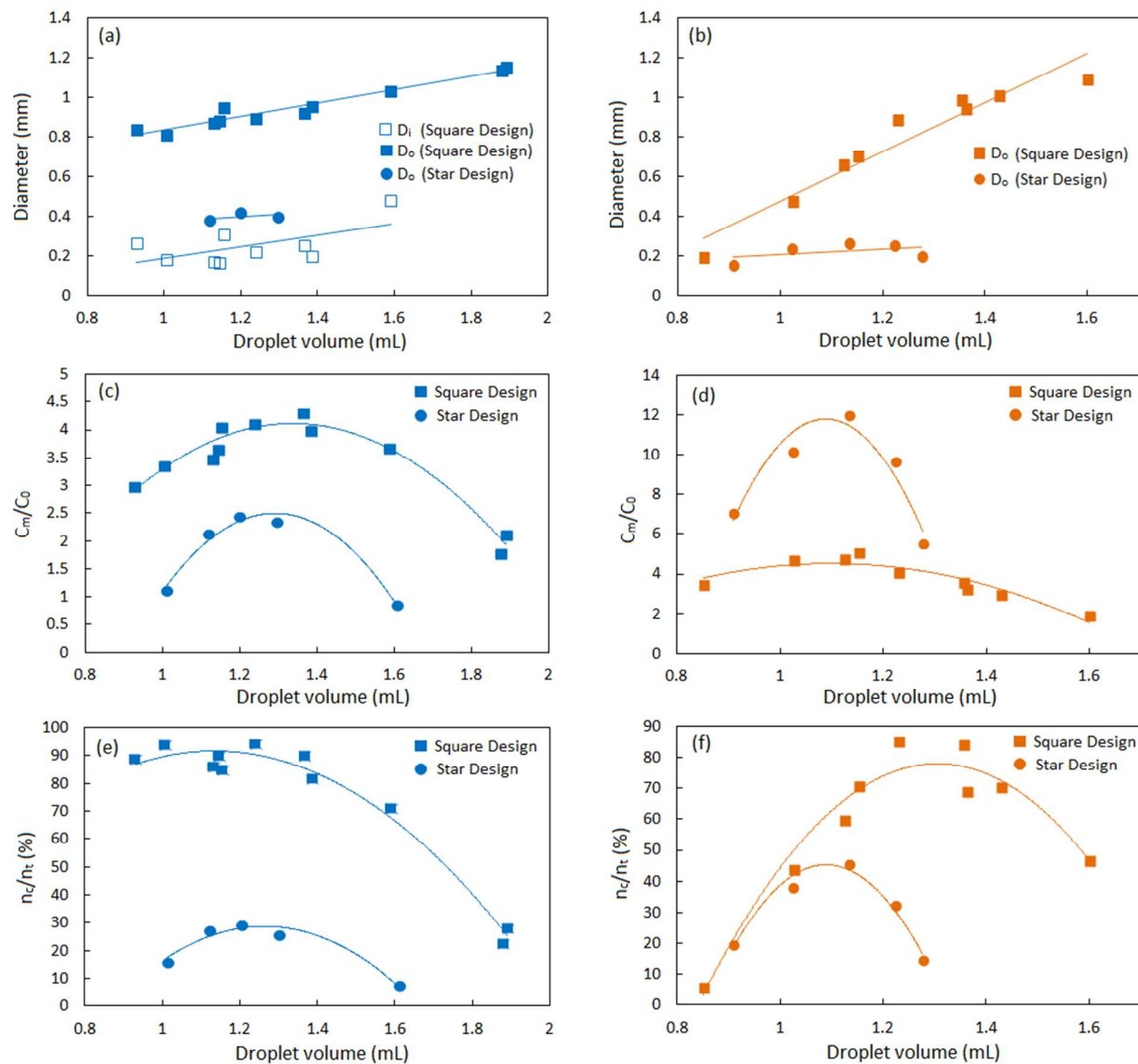
4

Fig 5 Effects of droplet volume on the behavior of particle-focusing for both Star design (circle markers) and the Square design (square markers). a) Diameters of the focused region versus the droplet volume for PS-15, b) Diameter of the focused region versus the droplet volume for Si-5, c) C_m/C_0 for PS-15 particle, d) C_m/C_0 for Si-5 particle, e) Capturing efficiency (n_c/n_t) for PS-15 and f) Capturing efficiency (n_c/n_t) for Si-5, versus the volume of the droplet.

5